ACS OMEGA

http://pubs.acs.org/journal/acsodf

Article

Effect on the Surface Anticorrosion and Corrosion Protection Mechanism of Integrated Rust Conversion Coating for Enhanced Corrosion Protection

Pengfei Yu, Yun Lei,* Zhaolin Luan, Yonggang Zhao, and Haoping Peng*

Cite This: *ACS Omega* 2022, 7, 8995−9003

Read Online

ACCESS | Metrics & More | Article Recommendations

ABSTRACT: Here, a series of integrated rust conversion agents/coatings were synthesized by esterification reaction of 3,4,5-trihydroxybenzoic acid (GA) and triethanolamine (TE). The structural features, rust conversion ability, and corrosion resistance of the synthesized rust conversion agents/coatings were analyzed using the Fourier transform infrared tests, scanning electron microscopy tests, X-ray diffraction tests, and electrochemical measurements. It was found that when the mass ratio of TE and GA was 2:1, the synthesized rust conversion agent/coating has best rust conversion ability and anti-corrosion performance (i.e., corrosion current density 7.480 × 10^{-7} A/cm^2). In addition, different from the traditional coatings, the integrated rust conversion coating developed in this study combines the primer and topcoat of traditional coatings into one, which can significantly increase the on-site construction efficiency. Furthermore, a new rust conversion mechanism for the optimized rust conversion agent/coating was proposed. The phenolic hydroxyl functional groups in the rust conversion agent can well chelate with Fe^{2+}/Fe^{3+} in the original rust layer and then form macromolecular compounds and dense chelating films inside the coating, which tightly wraps rust and also prevents the penetration and diffusion of corrosive medium, making them lose the opportunity to interact with each other.

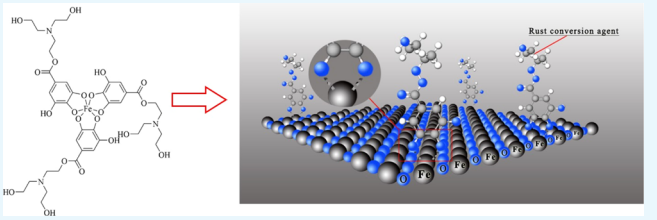

1. INTRODUCTION

The problem of metal corrosion is widespread in all aspects of social life, bringing great harm and loss to the development of various industries.[1] The research of the corrosion protection technology has always been valued by scientific researchers in various countries. According to reports, there are many methods to protect steel from corrosion, such as the organic coating,[2−5] inorganic coating,[6−8] nanocoating,[9−11] electrochemical protection,[12−14] and so on.[15−19] Among them, the organic coatings are the most widely used.

When using the traditional organic coatings, in order to achieve a better anti-corrosion effect, the strict surface rust removal treatment is necessary.[20] However, the pretreatment effect is often restricted by factors such as labor intensity, low efficiency, equipment location, and geometric shape, and it is often difficult to achieve the requirements of the standard Sa 2.5, resulting in the unguaranteed coating quality.[21,22] In addition, the traditional organic coatings often need to contain composite anticorrosive pigments such as the lead oxide and chromate, which have good anticorrosive properties.[23] However, their high toxicity is likely to cause harm to the environment and human health.[24,25] Therefore, it is vital to develop economical, safe, and environmentally friendly rust conversion agents and corresponding coatings,[26−29] which can be directly applied on the surface of the rust layer.

The traditional rust conversion agent is mainly based on tannic acid and phosphoric acid.[30−35] However, their significant problem is that the excessive acid introduced will bring a large number of active groups and reduce the coating stability and also further corrode the steel matrix. On the contrary, insufficient acid will bring incomplete rust conversion.[36,37] To this end, this research found that the 3,4,5-trihydoxybenzoic acid (GA) has many advantages to become an excellent rust conversion agent. First, it is widely present in grapes, tea, gallnut, bean pods, and other plants, and more importantly, its price is low; second, it is a kind of weak organic acid, and there is no problem of excessive corrosion of steel to some extent; and third, it contains three hydroxyl functional groups that can flexibly carry out certain reactions to strengthen its rust conversion ability. However, its low solubility limits its wide and effective application.[38,39] In order to make up for the shortcomings of GA and strengthen its application, this research first found that by modifying the GA into an ester using triethanolamine (TE), its product has

Received: January 9, 2022
Accepted: February 21, 2022
Published: March 1, 2022

https://doi.org/10.1021/acsomega.2c00172
ACS Omega 2022, 7, 8995−9003

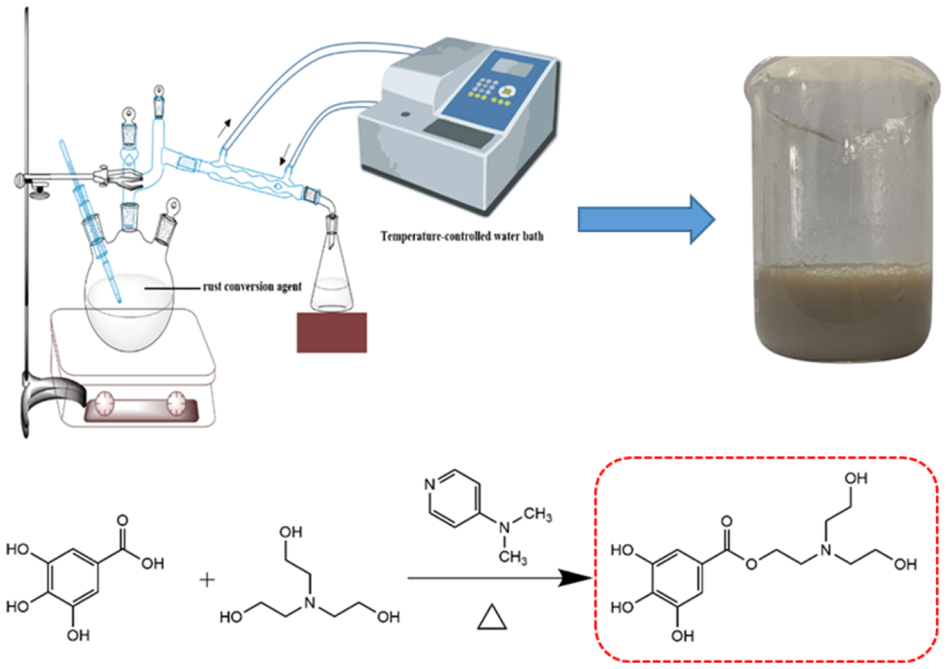

Figure 1. Synthesis reaction description of the rust conversion agent TE-GAE.

excellent solubility and rust conversion ability. As far as we know, there are few reports on using the GA ester (GAE) as a rust conversion agent.

The aim of this study is to prepare water-based rust conversion agents by the esterification reaction of TE and GA. By optimizing and changing the mass ratio of TE and GA, the optimized rust conversion agent is obtained. The synthesis and structure of the optimized rust conversion agent were confirmed by Fourier transform infrared (FTIR). Then, the scanning electron microscopy (SEM) and X-ray diffraction (XRD) were used to study the rust conversion ability of the rust conversion agent. Finally, the corrosion resistance of the rust conversion coating containing the optimized rust conversion agent was studied by the electrochemical test. The results show that the synthesized rust conversion agent/coating in this research has excellent rust conversion ability and corrosion resistance.

2. EXPERIMENTAL SECTION

2.1. Experimental Materials. All materials, such as the GA, 4-dimethylaminopyridine (DMAP), TE, ethanol, curing agent, and so forth, were purchased from Sinopharm Chemical Reagent Co., Ltd. (China). All chemicals used in this study are of analytical grade.

2.2. Synthesis of Rust Conversion Agent. The synthetic process of the rust conversion agent TE-GAE is shown in Figure 1. In the process, many proportioned TE-GAE rust conversion agents were synthesized under the condition of a different mass ratio of TE and GA. Here, four mass ratios of TE and GA were selected in this study, and the mass ratios of TE and GA were 1:1, 2:1, 3:1, and 4:1. In addition, DMAP is used as the catalyst. Taking the mass ratio of TE to GA 2:1 as an example, please refer to our previous article for the detailed preparation process.[40]

2.3. Preparation of Rust Samples Coated with Rust Conversion Coating. In this study, 20# steel was chosen as the rusted substrate. Before using, it was polished with 80, 250, and 1000 mesh sandpaper, then washed with pure ethanol, and finally dried. After this, it was exposed to the air for 60 days to make it rust evenly for use. For rusty 20# steel samples, a metal brush is used to roughly remove surface floating rust and dust, they are cleaned with pure ethanol, and then kept dried. After this, the rust conversion coating was directly and uniformly coated on the pretreated rust plate at one time. For the specific coating method and process, please refer to our previous published article.[40] The well-coated samples were dried in a drying oven at room temperature for 72 h, and then, the properties of the well-coated samples were analyzed by FTIR, SEM, potentiodynamic polarization (PDP), and electrochemical impedance spectroscopy (EIS).

2.4. Instrumentations and Characterization. In this study, an FTIR spectrometer (Thermo, USA) was used to obtain the FTIR spectra. During the testing process, the scanning wavenumber was set from 4000 to 400 cm^{-1}, and the tests were carried out at room temperature. In addition, the fracture surface morphology and microstructure of the prepared samples were obtained by SEM (HITACHI S4800). The electrochemical properties of the prepared samples were analyzed using the PDP test and EIS in 3.5 wt % NaCl solution on a CHI-660E electrochemical workstation (Chenhua, China) during many days of immersion, and for specific test methods, please refer to ref 40.

3. RESULTS AND DISCUSSION

3.1. Characterization of the As-Synthesized Rust Conversion Agent. In order to verify the production of the target product, Figure 2 displays the FT-IR spectra of the as-synthesized rust conversion agents in various mass ratios of TE and GA. Figure 2a–d respectively corresponds to the as-synthesized rust conversion agent products when the mass ratios of TE and GA are 1:1, 2:1, 3:1, and 4:1.

It can be seen from Figure 2a,c,d that there is no characteristic peak of the ester carbonyl −C═O at the corresponding ratio 1:1, 3:1, and 4:1 of TE and GA, indicating

https://doi.org/10.1021/acsomega.2c00172
ACS Omega 2022, 7, 8995−9003

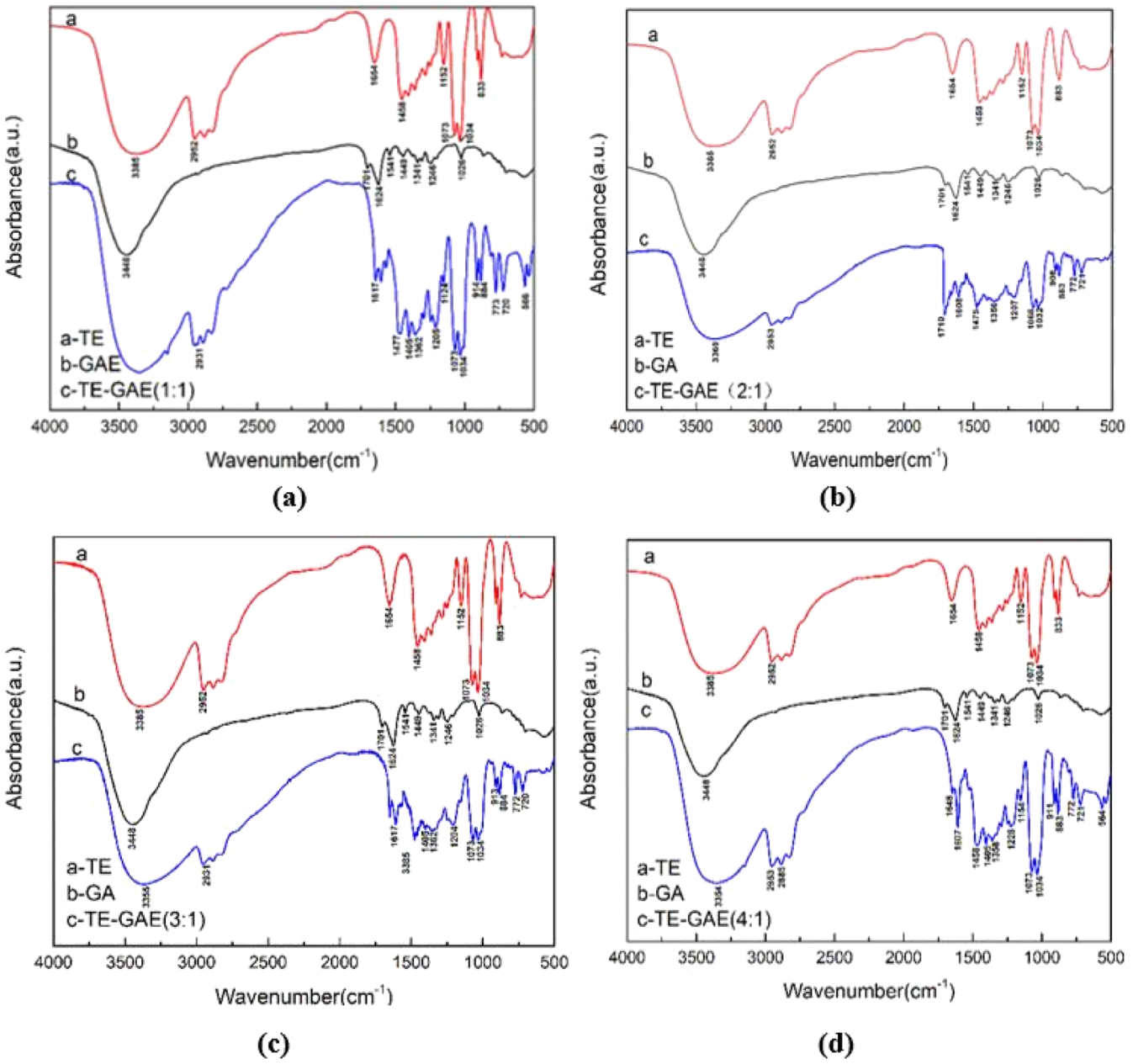

Figure 2. FT-IR spectra of TE, GA, and as-synthesized rust conversion agents with the TE and GA mass ratios of 1:1 (a), 2:1 (b), 3:1 (c), and 4:1 (d).

that the target product is not well generated. In these cases, because the TE or GA is in an excessive state, the target product cannot be completely idealized. Moreover, we found that when the mass ratio of TE and GA is 1:1, 3:1, and 4:1, the color of the product becomes lighter. In such cases, GA can react completely, but the unreacted TE in the whole system increases. At reaction temperatures, many hydrogen atoms on the hydroxyl groups in TE are replaced by aryl groups and etherified, which is also confirmed by the formation of ether bonds on the FITR spectra.

However, it can be seen from Figure 2b that at the position of 1710 cm^{-1}, the ester carbonyl −C═O stretching vibration absorption peak is clearly generated,[41] and the −C−O bond stretching vibration at 1207 cm^{-1} is also observed in the ester group. In Figure 2b, further study found that compared with the TE and GA, for the TE-GAE (2:1), the position and intensity of some absorption peaks have changed significantly. For example, at 3360 cm^{-1}, a strong peak is caused by −O−H stretching vibration.[42] In addition, we can find that the peaks at the positions of 2952, 2953⁻, and 1207 cm^{-1} correspond to the −C−H stretching vibration peak in the $-CH_3$ and $-CH_2$ groups.[43,44] In addition to this, the −C−N stretching vibration peak is also observed at 1475 cm^{-1}, and the absorption peaks of the substituted benzene ring in TE-GAE are between 772 and 721 cm^{-1}, which is consistent with ref 45. Moreover, a bending vibration peak in the -O-H plane appears at 1356 cm^{-1}. That is to say, when the mass ratio of TE to GA is 2:1, the formation of the rust conversion agent TE-GAE is good.

3.2. Analysis of the Rust Conversion Ability. *3.2.1. Analysis of the Color Change Degree of the Rust Layer.* An important criterion for measuring the quality of the rust conversion agent is the degree of rust conversion, and the

https://doi.org/10.1021/acsomega.2c00172
ACS Omega 2022, 7, 8995−9003

degree of blackening of the rust layer after applying rust conversion agents can explain this problem to a certain extent.[46] It can be seen in Figure 3 that after the rust

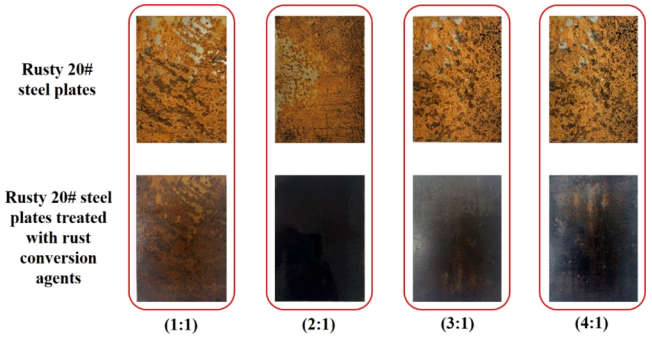

Figure 3. Analysis of the rust conversion degree under different rust conversion agents.

conversion agents are well coated on the surface of the rusty 20# steel plate for about 20 min, the surface morphology of the rusty 20# steel plate has changed significantly. According to the research of Gust et al., the change in the surface color of the rusty steel plate largely relies on the reaction between the rust and rust conversion agent to form other harmless substances.[46] In other words, the conversion degree of the rust conversion agent can be qualitatively reflected from the change degree in the color of the original rust layer.

When the mass ratio of TE and GA is 1:1, the surface color of the rust is almost unchanged, which means that the rust conversion agent almost does not react with the rust. Obviously, this situation is due to the fact that no effective rust conversion agent is produced. In addition, with the mass ratio of TE and GA reaching 3:1 and 4:1, the color of the original rusty sheet has changed significantly, but the treated surface shows obvious roughness and unevenness. On the one hand, it shows that a certain amount of the rust conversion agent is generated in this case, which causes the color of the original rust layer to change. On the other hand, since the TE content is excessive in these two cases, there are some free states of TE in the rust conversion agent system, resulting in the rust conversion agent not being quickly and completely solidified. During the curing process, there are bubbles oozing out from the rust conversion agent system. Meanwhile, the presence of the excessive TE results in poor leveling of the rust conversion agent to a certain extent. The above-mentioned two reasons cause the rusty surface to be rough and uneven.

In contrast, when the mass ratio of TE and GA is 2:1, after the rust conversion agent is well coated on the original rusty surface, it can be seen that a dense and shiny black protective film is formed on the rusty surface, which also indicates that the rust conversion agent can react strongly with rust in some way. In other words, the degree of rust conversion is the most obvious in this case, and the protective film produced is smooth and flat, which is also consistent with the results of FTIR.

3.2.2. Analysis of the Microstructure of the Rust Layer. The microstructure of the rusted surface after being treated using the rust conversion coatings from the perspective of SEM was also analyzed to illustrate the rust conversion ability.

It can be seen in Figure 4a that the original rust consists of fine particles and pores of different sizes. XRD test results found that it mainly consists of the α-FeOOH and γ-FeOOH

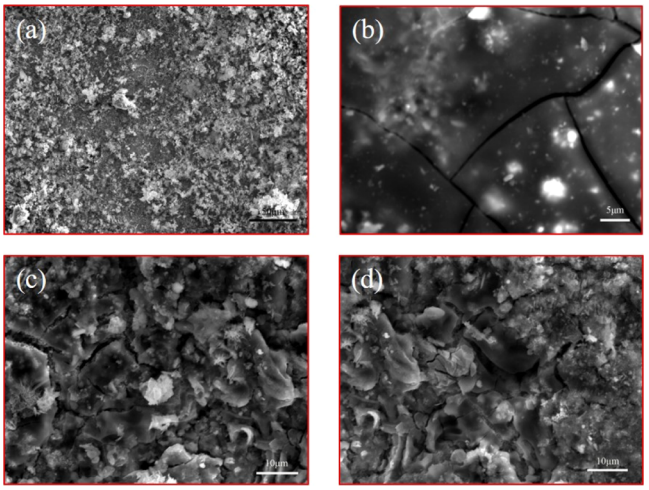

Figure 4. SEM results of the rusty surface before and after being treated using rust conversion agents.

(shown in Figure 5), which is the original appearance of the rusty 20# steel plate.[47] When the mass ratio of TE and GA is

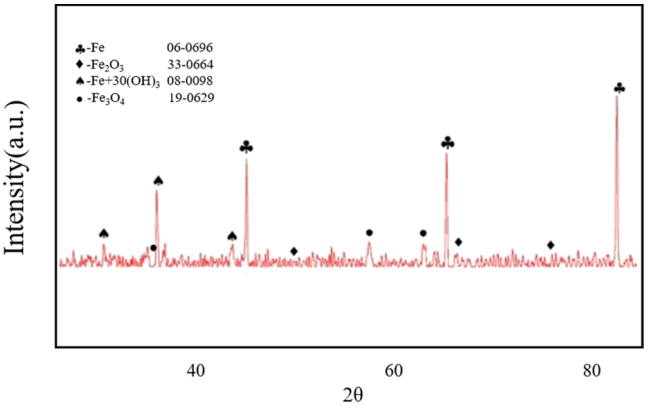

Figure 5. XRD result for the original rust.

2:1 (Figure 4b), the surface crystalline form of the rusted 20# steel plate disappears, and the surface morphology is transformed into a dense crack layer with accompanying bright particles of different shapes and sizes. Compared with the original rust layer, the porous and rough crystal shape almost all disappears, and the surface becomes smoother and more complete.

However, when the mass ratios of TE and GA are 3:1 (Figure 4c) and 4:1 (Figure 4d), α-FeOOH can still be seen in the rust layer after the rust conversion agent acts. This is due to the excessive TE in the rust conversion agent which results in poor leveling and permeability of the rust conversion agent, which means that it cannot well penetrate into the rust layer, resulting in only partial conversion of the rust and still a part of rust exposed to external conditions. In this case, the rust conversion effect is poor.

3.3. Electrochemical Polarization Measurements. The polarization curves of the rusted steel and rusted steel plates treated using the rust conversion coatings are shown in Figure 6. In addition, Table 1 gives the corrosion potential (E_{corr}) and corrosion current density (I_{corr}) obtained from the standard Tafel polarization section.

https://doi.org/10.1021/acsomega.2c00172
ACS Omega 2022, 7, 8995−9003

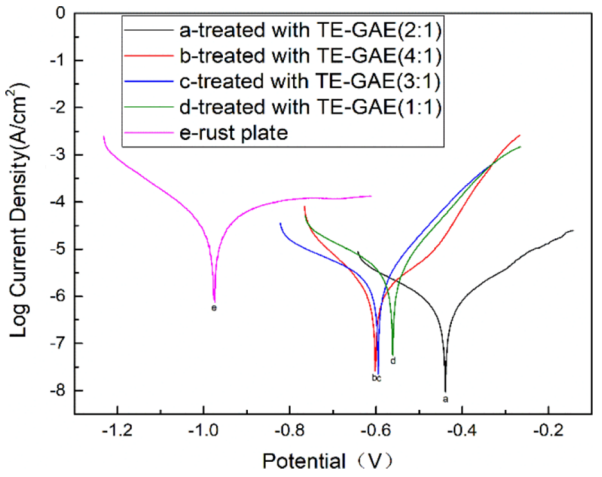

Figure 6. Tafel curves of untreated and treated rusted steels using rust conversion coatings.

Table 1. Electrochemical Test Results Obtained from Tafel Plots in Figure 6

specimens	E_{corr} (V)	I_{corr} (A/cm^2)	β_a	β_c
rusty steel plate	−0.974	3.557×10^{-5}	6.934	7.116
TE-GAE (1:1)	−0.561	3.413×10^{-6}	10.408	5.134
TE-GAE (2:1)	−0.439	7.480×10^{-7}	6.157	5.321
TE-GAE (3:1)	−0.602	1.449×10^{-6}	6.727	8.513
TE-GAE (4:1)	−0.595	2.371×10^{-6}	10.524	4.375

Compared to the curve for the rusted steel untreated with TE-GAE, it can be seen that the polarization curves of the rusted steels treated using TE-GAE clearly shift in the right down direction, which indicates that the driving force in the corrosion process is weakened. The I_{corr} of all treated samples is less than that of the untreated mildly rusted steel plate (3.557×10^{-5} A/cm^2), and the E_{corr} is greater than that of the untreated mildly rusted steel plate (−0.974 V), indicating that the coated samples have better corrosion resistance. Analysis of the reasons can be that this is mainly due to the chelation reaction between the rust conversion agent and the rust to form a stable protective film, which has a passivation effect.

In addition, it can be clearly seen that compared to other rust conversion agents [TE-GAE (3:1) and TE-GAE (4:1)], the rusted sample coated with TE-GAE (2:1) exhibits a minimum corrosion current density (7.480×10^{-7} A/cm^2) and a maximum corrosion potential (−0.439 V). Combining the previous rust conversion degree and surface microstructure, we believe that the improvement in corrosion performance is attributed to two aspects. First, at this ratio, the content of the rust conversion agent is the highest, and accordingly, the conversion effect of the original rust layer is the best. Second, under the continuous action of the rust conversion agent, the original loose rust is converted into harmless chelate fillers, making the entire rust layer more dense and complete. In this case, it is difficult for the corrosive medium enter into and come in contact with the steel substrate.

3.4. Electrochemical Impedance Measurement. The electrochemical equivalent circuit used in this study is shown in Figure 7. In this model, R_s is the electrolyte resistance, and R_c and C_c are the resistance and capacitance of the rust conversion coatings, respectively. In addition, typical EIS Nyquist and Bode plots for the untreated and treated rusted steels using rust conversion coatings during immersion in 3.5 wt % NaCl solution for 1 day are taken, as shown in Figures 8 and 9, respectively.

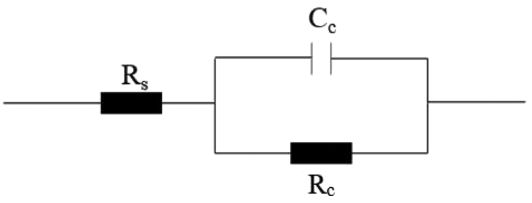

Figure 7. Electrochemical equivalent circuit used in this study.

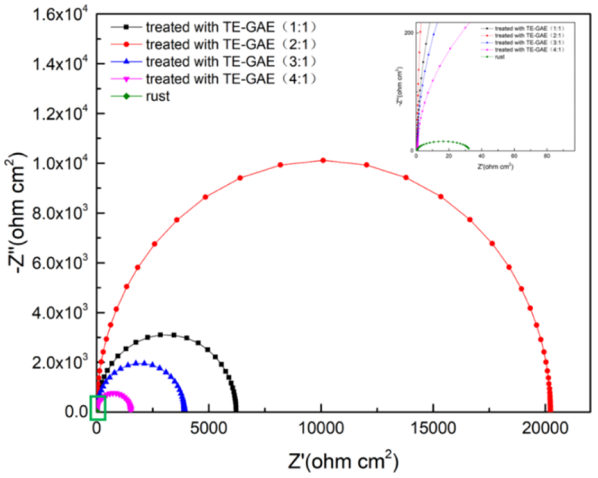

Figure 8. EIS Nyquist diagrams of rusted steels treated with/without rust conversion coatings. Symbol: experimental data, line: fitted data.

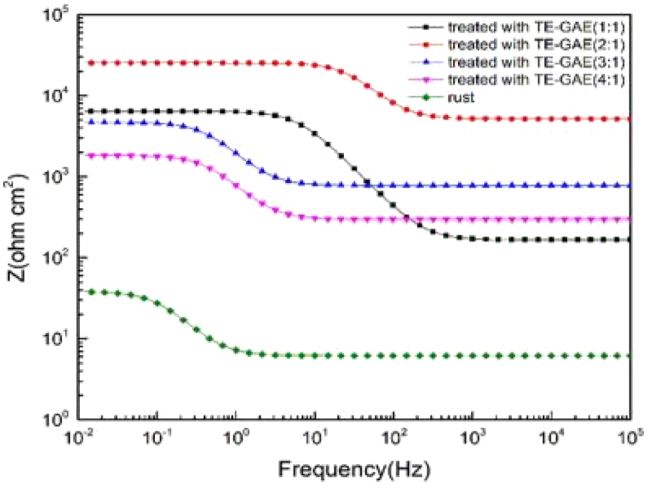

Figure 9. EIS Bode diagrams of rusty 20# steel treated with rust conversion coatings. Symbol: experimental data, line: fitted data.

Compared with the untreated rusted steels using rust conversion coatings, the corrosion resistance of the treated rusted steels has been significantly improved. It can be seen in Figure 8 that the rusted steel treated with TE-GAE (2:1) has the largest impedance radius and capacitance loop and only contains a time constant, which indicates that it shows the most excellent anti-corrosion performance. In this case, the chelate formed between the rust conversion agent and the rust is the most stable, and the film formation is the most complete. However, when the mass ratios of TE and GA are 1:1, 3:1, and

https://doi.org/10.1021/acsomega.2c00172
ACS Omega 2022, 7, 8995−9003

4:1, the rust conversion agent contains a large amount of the unreacted TE. As we know, because TE contains three hydrophilic hydroxyl groups, it is easily soluble in solvent water. In other words, the remaining TE in the conversion film will gradually dissolve during the whole immersion process. In this case, the dissolution of TE will inevitably affect the integrity and compactness of the whole rust conversion layer, and some defects will naturally appear. Once in contact with the corrosive medium, the corrosive medium will penetrate along the defect location and diffuse into the inside of the substrate, which results in the rust conversion layer to weaken and reduced corrosion resistance.

Meanwhile, the impedance modulus of the anti-corrosion coating at low frequency of 0.01 Hz is recognized to reflect the anti-corrosion performance. The larger the value, the better the early anti-corrosion performance.[48,49] According to the Bode plot in Figure 9, we can find that for the rusted steels that have not been treated with the rust conversion agent, the low-frequency impedance value is very small, and it is in an unprotected state at this time. With the use of the rust conversion agent, the low-frequency impedance values of the rusty samples have changed significantly in magnitude. This also shows that the use of the rust conversion agents has a significant protective effect on the rusty samples and enhances its corrosion resistance. In addition, compared with the use of other rust conversion agents [TE-GAE (3:1) and TE-GAE (4:1)], when the rust sample is treated with the rust conversion agent TE-GAE (2:1), its low-frequency impedance value reaches the order of 10^4 to 10^5 Ω·cm^2, which is much higher than other cases. In other words, the rust conversion layer formed in this case has the best protective effect, which is also consistent with the test result of the Tafel curve.

In order to further illustrate the performance of the rust conversion coating TE-GAE (2:1), this study separately treated the rusted steel using the rust conversion coating TE-GAE (2:1) and then measured the electrochemical spectra under different immersion times. Figure 10 shows the results of Nyquist diagrams.

Obviously, it can be seen from Figure 10 that with the increase in the immersion time, the capacitive loop kept shrinking, and the semicircle diameter kept decreasing, which indicates that the resistance of the rust sample decreases during the immersion process. In addition, after immersion for 30 days, the Nyquist diagram still shows a single capacitance arc, and the shape hardly did not change significantly. However, compared to the case of immersion for 1 day, the reduction in the impedance modulus is still very significant, exceeding 2 orders of magnitude. However, on the other hand, for the cases of immersion for 14 days and 30 days, the impedance modulus of the two is relatively close. This phenomenon explains at least two problems. One is that the corrosion mechanism has not changed during the entire immersion, and the other is that the anti-corrosion properties of the coating formed by a single rust conversion agent are still not durable in the short term. With the continuous intrusion of corrosive medium, the rust conversion layer with anti-corrosion properties is continuously destroyed. However, with the continuous action of the rust conversion agent, the anti-corrosion properties of the entire sample will not continually deteriorate and gradually reach stability in the long term. Of course, we all know that a qualified anti-corrosion coating must also contain other additives, such as film formers, dispersants, and so forth.

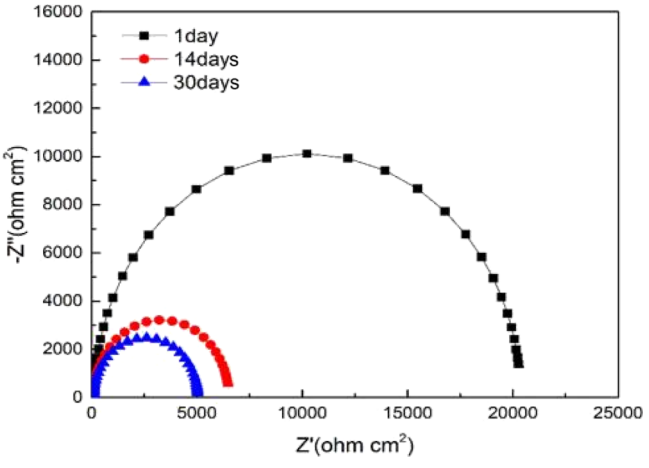

Figure 10. EIS Nyquist diagrams of rusted steel treated using the rust conversion coating containing the TE-GAE (2:1) after immersion of 1, 14, and 30 days. Symbol: experimental data, line: fitted data.

Figure 11 shows the Bode diagram of the rust sample treated with the rust conversion agent TE-GAE (2:1). Generally, as

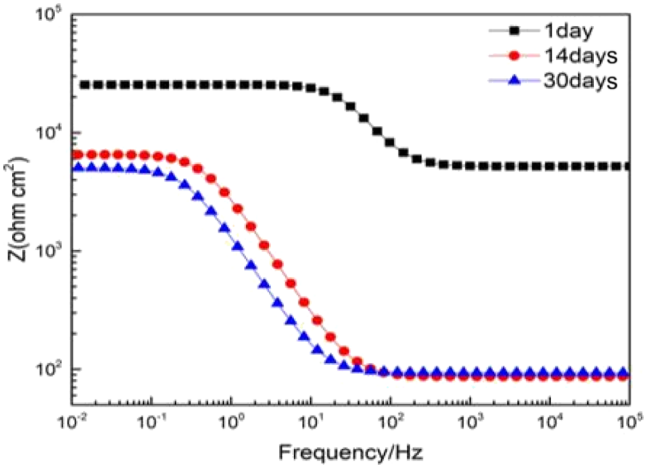

Figure 11. EIS Bode diagrams of rusted steel treated using the rust conversion coating containing the TE-GAE (2:1) after immersion of 1, 14, and 30 days. Symbol: experimental data, line: fitted data.

immersion time increases, the impedance modulus kept decreasing, but the decrease magnitude of the impedance modulus gradually decreases. Moreover, after 14 days and 30 days of immersion, the impedance modulus of the two samples is very close, which shows that the impedance of the rust conversion layer has basically reached a stable level. This is consistent with the results of the Nyquist diagrams.

3.5. Mechanism of Rust Conversion and Anti-corrosion of Rust Conversion Coating. In order to explore the mechanism of rust conversion and anti-corrosion of the integrated rust conversion coating, this study further analyzed the FTIR spectra of original rust and rust treated using the rust conversion coating, as shown in Figure 12.

It is obvious that for the rust in Figure 12a, the peak at 3448 cm^{-1} corresponds to the peak of −O−H tensile vibration. In addition, the absorption peaks of γ-FeOOH at 1021 cm^{-1} and Fe_3O_4 at 546 cm^{-1} can be observed. In addition to this, at 1654 cm^{-1}, the tensile vibration peak of α-FeOOH is also observed. On comparing Figure 12b with Figure 12a, it can be seen that

https://doi.org/10.1021/acsomega.2c00172
ACS Omega 2022, 7, 8995−9003

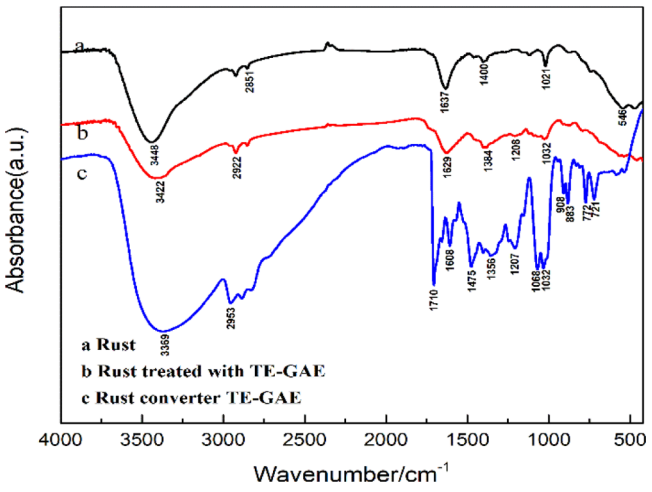

Figure 12. FT-IR spectra: (a) original rust; (b) rust treated with TE-GAE; and (c) rust converter TE-GAE.

the absorption peaks of γ-FeOOH at 1021 cm^{-1} and Fe_3O_4 at 546 cm^{-1} disappeared. Meanwhile, the tensile vibration peak of α-FeOOH at 1654 cm^{-1} is also weakened or even disappeared. However, we can clearly find that the strong peak of −O−H at 3448 cm^{-1} in Figure 12a is weakened, and it is transferred to the position of 3422 cm^{-1} in Figure 12b, which means the decrease in −O−H, indicating that certain chelate reactions take place between the rust conversion agent and Fe^{2+}/Fe^{3+}. In this case, the γ-FeOOH, Fe_3O_4, and α-FeOOH in original rust can be converted to form some large chelates, preventing further diffusion of rust. On further comparing Figure 12b with Figure 12c, it is found that the peak intensity of −O−H at 3369 cm^{-1} is significantly weakened, and two new peaks are generated at 1208 and 1384 cm^{-1}. In addition, the disappearance of the stretching vibration peak of −C−N at 1475 cm^{-1} indicates that the lone pair of electrons on the N atom can act with Fe^{2+}/Fe^{3+} to form a new bond, which further strengthens the stability of the formed chelate with the Fe−O−C bond.

Based on the FT-IR result, the following mechanism of the rust conversion coating is proposed, as shown in Figure 13. First, the rust conversion agent contains three phenolic hydroxyl functional groups, of which the oxygen atoms in the two phenolic hydroxyl functional groups contain two lone pairs of electrons. By interacting with electrons on the d orbital of iron atoms, it can well chelate with Fe^{2+}/Fe^{3+} in the form of Fe−O−C bonds to form macromolecular compounds, which have a stable six-member network structure and are densely distributed on the rust layer inside. Second, the remaining phenolic hydroxyl group in the rust conversion agent can also cooperate with the lone pair of electrons on the N atom to chelate with Fe^{2+}/Fe^{3+}, which further enhances the stability of the converted product.

Once the above-mentioned action mechanism has occurred, it will inevitably bring two results. On the one hand, the iron ions in original rust will be tightly bound inside the rust conversion agent, making them lose the opportunity to interact with corrosive medium. On the other hand, the entire original rust layer will be tightly wrapped as harmless fillers by the rust conversion agent and form macromolecular iron compounds. As shown in Figure 14, it can be seen that after being treated

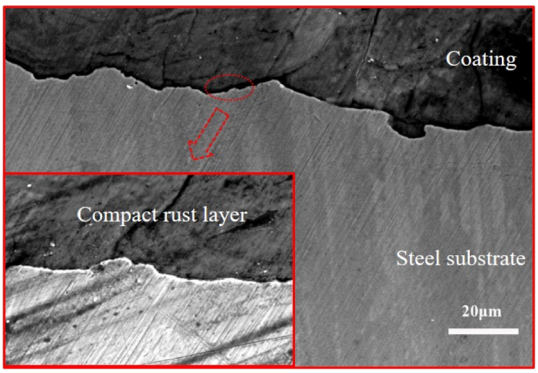

Figure 14. Cross-sectional morphology after treatment with rust conversion coating.

with the rust conversion agent, it converts the original layer from a porous structure to a plane dense structure. In other words, the formation with plane dense structure compounds makes the entire surface and cross-sectional morphology smooth and compact, and the defect locations are significantly reduced. In such case, the diffusion path of corrosive medium is lengthened and prevented.

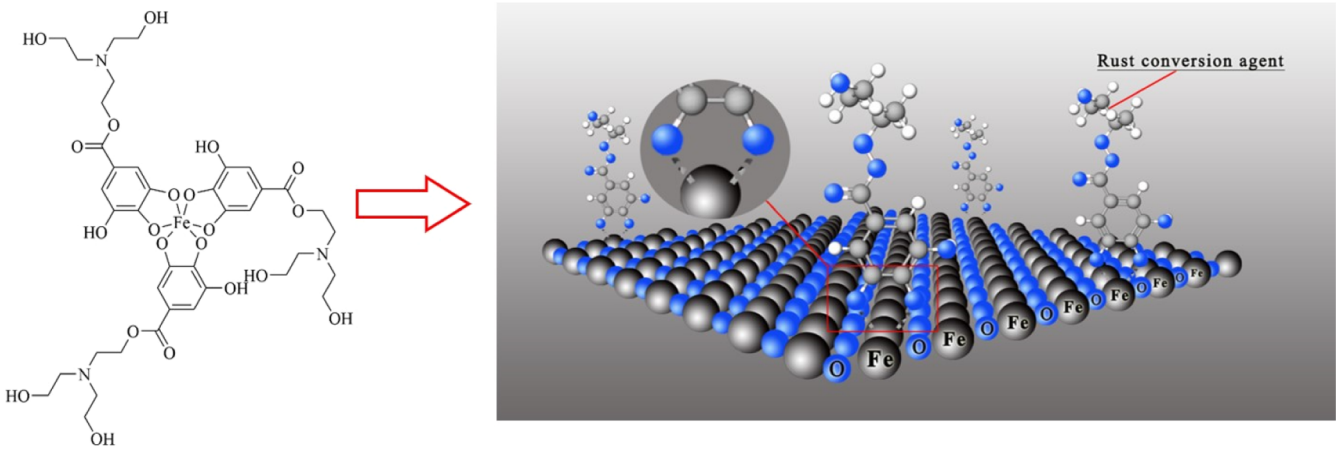

Figure 13. Anti-corrosion mechanism of the rust conversion agent.

https://doi.org/10.1021/acsomega.2c00172
ACS Omega 2022, 7, 8995−9003

4. CONCLUSIONS

A water-based, eco-friendly, and high-efficiency integrated rust conversion agent/coating was successfully synthesized, which has excellent chelating ability, rust conversion ability, and corrosion resistance. FT-IR results showed that the rust conversion agent can chelate with Fe^{2+}/Fe^{3+} in original rust to form stable macromolecular iron compounds containing Fe−O−C bonds, which effectively prevented corrosive medium from entering the steel matrix. SEM results show that the loose and porous rust layer is transformed into compact and flat compounds after being treated with the rust conversion agent, and the content of α-FeOOH and γ-FeOOH in original rust is significantly reduced, indicating that the conversion effect of the rust conversion agent/coating is remarkable. Meanwhile, the rust conversion agent has better permeable ability, which can well enter into the original rust layer and wrap the original rust. Therefore, the rust conversion agent/coating improves the adhesion and corrosion resistance of rusty steel and can be used to make multi-purpose composite coatings.

AUTHOR INFORMATION

Corresponding Authors

Yun Lei − *Jiangsu Key Laboratory of Oil and Gas Storage & Transportation Technology, Changzhou University, Jiangsu 213164, China*; Email: leiy@cczu.edu.cn

Haoping Peng − *Jiangsu Key Laboratory of Oil and Gas Storage & Transportation Technology, Changzhou University, Jiangsu 213164, China; Jiangsu Key Laboratory of Material Surface Science and Technology and Jiangsu Collaborative Innovation Center of Photovoltaic Science and Engineering, Changzhou University, Jiangsu 213164, China*; Email: php@cczu.edu.cn

Authors

Pengfei Yu − *Jiangsu Key Laboratory of Oil and Gas Storage & Transportation Technology, Changzhou University, Jiangsu 213164, China*; orcid.org/0000-0002-3859-4540

Zhaolin Luan − *Jiangsu Key Laboratory of Oil and Gas Storage & Transportation Technology, Changzhou University, Jiangsu 213164, China; CNOOC Changzhou Paint and Coatings Industry Research Institute, Changzhou 213000 Jiangsu, China*

Yonggang Zhao − *Jiangsu Key Laboratory of Oil and Gas Storage & Transportation Technology, Changzhou University, Jiangsu 213164, China; Corrosion and Protection Center, Institute for Advanced Materials and Technology, University of Science and Technology Beijing, Beijing 100083, China*

Complete contact information is available at: https://pubs.acs.org/10.1021/acsomega.2c00172

Notes

The authors declare no competing financial interest.

ACKNOWLEDGMENTS

This work was supported by the National Natural Science Foundation of China (grant no. 52174057) and the Science and Technology Project of Changzhou City (grant no. CJ20210136).

REFERENCES

(1) Bhaskaran, R.; Palaniswamy, N.; Rengaswamy, N. S.; Jayachandran, M. A review of differing approaches used to estimate the cost of corrosion (and their relevance in the development of modern corrosion prevention and control strategies). *Anti-Corros. Methods Mater.* **2005**, *52*, 29−41.

(2) Govindaraju, K. M.; Prakash, V. C. A. Synthesis of zinc modified poly(aniline-co-pyrrole) coatings and its anti-corrosive performance on low nickel stainless steel. *Colloids Surf., A* **2015**, *465*, 11−19.

(3) Zhang, R. F.; Zhang, S. F.; Xiang, J. H.; Zhang, L. H.; Zhang, Y. Q.; Guo, S. B. Influence of sodium silicate concentration on properties of micro arc oxidation coatings formed on AZ91HP magnesium alloys. *Surf. Coat. Technol.* **2012**, *206*, 5072−5079.

(4) Chen, C.; Qiu, S.; Cui, M.; Qin, S.; Yan, G.; Zhao, H.; Wang, L.; Xue, Q. Achieving high performance corrosion and wear resistant epoxy coatings via incorporation of noncovalent functionalized graphene. *Carbon* **2017**, *114*, 356−366.

(5) Mahmood, H.; Vanzetti, L.; Bersani, M.; Pegoretti, A. Mechanical properties and strain monitoring of glass-epoxy composites with graphene-coated fibers. *Composites, Part A* **2018**, *107*, 112−123.

(6) Zhang, X.; Liang, J.; Liu, B.; Peng, Z. Preparation of superhydrophobic zinc coating for corrosion protection. *Colloids Surf., A* **2014**, *454*, 113−118.

(7) Sun, C.; Zeng, H.; Luo, J.-L. Unraveling the effects of CO2 and H2S on the corrosion behavior of electroless Ni-P coating in CO2/H2S/Cl- environments at high temperature and high pressure. *Corros. Sci.* **2019**, *148*, 317−330.

(8) Usman, B. J.; Gasem, Z. M.; Umoren, S. A.; Solomon, M. M. Eco-friendly 2-Thiobarbituric acid as a corrosion inhibitor for API 5L X60 steel in simulated sweet oilfield environment: electrochemical and surface analysis studies. *Sci. Rep.* **2019**, *9*, 830.

(9) Du, H.-Y.; An, Y.-L.; Wei, Y.-H.; Hou, L.-F.; Liu, B.-S.; Liu, H.; Ma, Y.; Zhang, J.-X.; Wang, N.; Umar, A.; Guo, Z.-H. Nickel powders modified nanocoating strengthened iron plates by surface mechanical attrition alloy and heat treatment. *Sci. Adv. Mater.* **2018**, *10*, 1063−1072.

(10) Cui, G.; Bi, Z.; Liu, J.; Wang, S.; Li, Z. New method for CO2 corrosion resistance Ni-W-Y2O3-ZrO2 nanocomposite coatings. *Ceram. Int.* **2019**, *45*, 6163−6174.

(11) Luo, X.; Zhong, J.; Zhou, Q.; Du, S.; Yuan, S.; Liu, Y. Cationic reduced graphene oxide as self-aligned nanofiller in the epoxy nanocomposite coating with excellent anticorrosive performance and its high antibacterial activity. *ACS Appl. Mater. Interfaces* **2018**, *10*, 18400−18415.

(12) Dwivedi, D.; Lepková, K.; Becker, T. Carbon steel corrosion: a review of key surface properties and characterization methods. *RSC Adv.* **2017**, *7*, 4580−4610.

(13) Qian, Y.; Li, Y.; Jungwirth, S.; Seely, N.; Fang, Y.; Shi, X. The application of anti-corrosion coating for preserving the value of equipment asset in chloride-laden environments: a review. *Int. J. Electrochem. Sci.* **2015**, *10*, 10756−10780.

(14) Dai, M.; Liu, J.; Huang, F.; Zhang, Y.; Cheng, Y. F. Effect of cathodic protection potential fluctuations on pitting corrosion of X100 pipeline steel in acidic soil environment. *Corros. Sci.* **2018**, *143*, 428−437.

(15) Redjdal, O.; Zaid, B.; Tabti, M. S.; Henda, K.; Lacaze, P. C. Characterization of thermal flame sprayed coatings prepared from FeCr mechanically milled powder. *J. Mater. Process. Technol.* **2013**, *213*, 779−790.

(16) Qiu, S.; Li, W.; Zheng, W.; Zhao, H.; Wang, L. Synergistic Effect of Polypyrrole-Intercalated Graphene for Enhanced Corrosion Protection of Aqueous Coating in 3.5% NaCl Solution. *ACS Appl. Mater. Interfaces* **2017**, *9*, 34294−34304.

(17) Du, Y.; Li, N.; Zhang, T.-L.; Feng, Q.-P.; Du, Q.; Wu, X.-H.; Huang, G.-W. Reduced graphene oxide coating with anticorrosion and electrochemical property-enhancing effects applied in hydrogen Storage System. *ACS Appl. Mater. Interfaces* **2017**, *9*, 28980−28989.

https://doi.org/10.1021/acsomega.2c00172
ACS Omega 2022, 7, 8995−9003

(18) Liu, J.; Yu, Q.; Yu, M.; Li, S.; Zhao, K.; Xue, B.; Zu, H. Silane modification of titanium dioxide-decorated graphene oxide nanocomposite for enhancing anticorrosion performance of epoxy coatings on AA-2024. *J. Alloys Compd.* **2018**, *744*, 728−739.
(19) Qi, K.; Sun, Y.; Duan, H.; Guo, X. A corrosion-protective coating based on a solution-processable polymer-grafted graphene oxide nanocomposite. *Corros. Sci.* **2015**, *98*, 500−506.
(20) Sekhavat Pour, Z.; Ghaemy, M.; Bordbar, S.; Karimi-Maleh, H. Effects of surface treatment of TiO2 nanoparticles on the adhesion and anticorrosion properties of the epoxy coating on mild steel using electrochemical technique. *Prog. Org. Coat.* **2018**, *119*, 99−108.
(21) Zhang, Y.; Yu, P.; Wu, J.; Chen, F.; Li, Y.; Zhang, Y.; Zuo, Y.; Qi, Y. Enhancement of anticorrosion protection via inhibitor-loaded ZnAlCe-LDH nanocontainers embedded in sol-gel coatings. *J. Coat. Technol. Res.* **2018**, *15*, 303−313.
(22) Roselli, S. N.; Romagnoli, R.; Deyá, C. The anti-corrosion performance of water-borne paints in long term tests. *Prog. Org. Coat.* **2017**, *109*, 172−178.
(23) Holmes, A. L.; Wise, S. S.; Sandwick, S. J.; Lingle, W. L.; Negron, V. C.; Thompson, W. D.; Wise, J. P. Chronic exposure to lead chromate causes centrosome abnormalities and aneuploidy in human lung cells. *Cancer Res.* **2006**, *66*, 4041−4048.
(24) Sanaei, Z.; Bahlakeh, G.; Ramezanzadeh, B. Active corrosion protection of mild steel by an epoxy ester coating reinforced with hybrid organic/inorganic green inhibitive pigment. *J. Alloys Compd.* **2017**, *728*, 1289−1304.
(25) Sanaei, Z.; Ramezanzadeh, B.; Shahrabi, T. Anti-corrosion performance of an epoxy ester coating filled with a new generation of hybrid green organic/inorganic inhibitive pigment; electrochemical and surface characterizations. *Appl. Surf. Sci.* **2018**, *454*, 1−15.
(26) Bera, S.; Rout, T. K.; Udayabhanu, G.; Narayan, R. Water-based & eco-friendly epoxy-silane hybrid coating for enhanced corrosion protection & adhesion on galvanized steel. *Prog. Org. Coat.* **2016**, *101*, 24−44.
(27) Cai, K.; Zuo, S.; Luo, S.; Yao, C.; Liu, W.; Ma, J.; Mao, H.; Li, Z. Preparation of polyaniline/graphene composites with excellent anti-corrosion properties and their application in waterborne polyurethane anticorrosive coatings. *RSC Adv.* **2016**, *6*, 95965−95972.
(28) Christopher, G.; Anbu Kulandainathan, M.; Harichandran, G. Comparative study of effect of corrosion on mild steel with waterborne polyurethane dispersion containing graphene oxide versus carbon black nanocomposites. *Prog. Org. Coat.* **2015**, *89*, 199−211.
(29) Wang, N.; Zhang, Y.; Chen, J.; Zhang, J.; Fang, Q. Dopamine modified metal-organic frameworks on anti-corrosion properties of waterborne epoxy coatings. *Prog. Org. Coat.* **2017**, *109*, 126−134.
(30) Achmad, A.; Kassim, J.; Ghafli, A. U.; Hamdan, H. Mangrove tannin (Rhizophora apiculata) complexes with copper (II) ion as an antifoulant in antifouling paint for fish net. *Adv. Mater. Res.* **2014**, *1043*, 204−208.
(31) Cruz, B. H.; Díaz-Cruz, J. M.; Ariño, C.; Esteban, M. Heavy Metal Binding by Tannic Acid: A Voltammetric Study. *Electroanalysis* **2000**, *12*, 1130−1137.
(32) Hornus Sack, S.; Romagnoli, R.; Vetere, V. F.; Elsner, C. I.; Pardini, O.; Almalvy, J. I.; Sarli, A. R. D. Evaluation of steel/primer based on chestnut tannin/paint film systems by EIS. *J. Coat. Technol.* **2002**, *74*, 63−69.
(33) Martinez, S. Inhibitory mechanism of mimosa tannin using molecular modeling and substitutional adsorption isotherms. *Mater. Chem. Phys.* **2003**, *77*, 97−102.
(34) Martinez, S.; Stern, I. Thermodynamic characterization of metal dissolution and inhibitor adsorption processes in the low carbon steel/mimosa tannin/sulfuric acid system. *Appl. Surf. Sci.* **2002**, *199*, 83−89.
(35) Pardini, O. R.; Amalvy, J. I.; Sarli, A. R.; Romagnoli, R.; Vetere, V. F. Formulation and testing of a waterborne primer containing chestnut tannin. *J. Coat. Technol.* **2001**, *73*, 99−106.
(36) Cui, G.; Bi, Z.; Zhang, R.; Liu, J.; Yu, X.; Li, Z. A comprehensive review on graphene-based anti-corrosive coatings. *Chem. Eng. J.* **2019**, *373*, 104−121.
(37) Lei, Y.; Xiao, W.; Peng, H.; Yu, P.; Cai, X.; Luan, Z.; Deng, S.; Wang, S. An integrated epoxy rust conversion coating: Its anticorrosion properties and rust conversion mechanism. *J. Alloys Compd.* **2021**, *853*, 157005.
(38) Ocampo, L. M.; Margarit, I. C. P.; Mattos, O. R.; Córdoba-de-Torresi, S. I.; Fragata, F. L. Performance of rust converter based in phosphoric and tannic acids. *Corros. Sci.* **2004**, *46*, 1515−1525.
(39) Liu, S.; Gu, L.; Zhao, H.; Chen, J.; Yu, H. Corrosion resistance of graphene-reinforced waterborne epoxy coatings. *J. Mater. Sci. Technol.* **2016**, *32*, 425−431.
(40) Lei, Y.; Yu, P.; Peng, H.; Luan, Z.; Deng, S.; Wang, S.; Zhou, N. Water-based & eco-friendly & high-efficiency 3,4,5-Trihydroxybenzoic acid ester as a novel rust conversion agent and its polymer composites for enhanced surface anticorrosion. *Colloids Surf., A* **2021**, *626*, 127065.
(41) Wang, H.; Zhou, Q. Synthesis of cardanol-based polyols via Thiol-ene/Thiol-epoxy dual click-reactions and thermosetting polyurethanes therefrom. *ACS Sustainable Chem. Eng.* **2018**, *6*, 12088−12095.
(42) Jiang, T.; Kuila, T.; Kim, N. H.; Ku, B.-C.; Lee, J. H. Enhanced mechanical properties of silanized silica nanoparticle attached graphene oxide/epoxy composites. *Compos. Sci. Technol.* **2013**, *79*, 115−125.
(43) Wang, X.; Xing, W.; Zhang, P.; Song, L.; Yang, H.; Hu, Y. Covalent functionalization of graphene with organosilane and its use as a reinforcement in epoxy composites. *Compos. Sci. Technol.* **2012**, *72*, 737−743.
(44) Lin, Z.; Liu, W.; Tan, J. Properties of (meth)acrylate copolymer grafted with long fluorinated side chain prepared by "graft onto" strategy. *J. Appl. Polym. Sci.* **2018**, *135*, 45894.
(45) Jia, Y.; Ren, N.; Yue, H.; Deng, J.; Liu, Y. Preparation and properties of natural gallic acid based rust conversion emulsion. *Pigm. Resin Technol.* **2016**, *45*, 191−198.
(46) Gust, J.; Suwalski, J. Use of Mossbauer spectroscopy to study reaction products of polyphenols and iron compounds. *Corrosion* **2012**, *50*, 355−365.
(47) Barrero, C. A.; Ocampo, L. M.; Arroyave, C. E. Possible improvements in the action of some rust converters. *Corros. Sci.* **2001**, *43*, 1003−1018.
(48) Li, Y.; Zhang, X.; Cui, Y.; Wang, H.; Wang, J. Anti-corrosion enhancement of superhydrophobic coating utilizing oxygen vacancy modified potassium titanate whisker. *Chem. Eng. J.* **2019**, *374*, 1326−1336.
(49) Xia, D.-H.; Song, S.; Qin, Z.; Hu, W.; Behnamian, Y. Review-Electrochemical Probes and Sensors Designed for Time-Dependent Atmospheric Corrosion Monitoring: Fundamentals, Progress, and Challenges. *J. Electrochem. Soc.* **2020**, *167*, 037513.

https://doi.org/10.1021/acsomega.2c00172
ACS Omega 2022, 7, 8995−9003